Structural polymorphism of α-synuclein fibrils alters pathway of Hsc70 mediated disaggregation

Svenja Jäger[1], Jessica Tittelmeier[1,2], Thi Lieu Dang[1], Tracy Bellande[3], Virginie Redeker[3], Alexander K. Buell[4], Ronald Melki[3*], Carmen Nussbaum-Krammer[1,2*], Bernd Bukau[1*] and Anne S. Wentink[1,5*]

[1] Center for Molecular Biology of Heidelberg University (ZMBH), DKFZ-ZMBH Alliance, Heidelberg, Germany.

[2] Chair of Neuroanatomy, Institute of Anatomy, Faculty of Medicine, Ludwig-Maximilians-University of Munich (LMU), Munich, Germany.

[3] Institute Francois Jacob (MIRCen), CEA, and Laboratory of Neurodegenerative Diseases, CNRS, Fontenay-Aux-Roses, France.

[4] Department of Biotechnology and Biomedicine, Technical University of Denmark (DTU), Kgs. Lyngby, Denmark.

[5] Leiden Institute of Chemistry (LIC), Leiden University, Leiden, Netherlands.

* Corresponding authors:
Anne S. Wentink: a.s.wentink@lic.leidenuniv.nl
Bernd Bukau: b.bukau@zmbh.uni-heidelberg.de
Carmen Nussbaum-Krammer: carmen.nussbaum@med.uni-muenchen.de
Ronald Melki: ronald.melki@cnrs.fr

Keywords: alpha-synuclein/ polymorphism /disaggregation / Hsp70/ molecular chaperones

Abstract

The pathological aggregation of α-synuclein into amyloid fibrils is a hallmark of synucleinopathies including Parkinson's disease. Despite this commonality, synucleinopathies display divergent disease phenotypes that have been attributed to disease specific three-dimensional structures of α-synuclein fibrils, each with a unique toxic gain-of-function profile. The Hsc70 chaperone is remarkable in its ability to disassemble pre-existing amyloid fibrils of different proteins in an ATP and co-chaperone dependent manner. We find however, using six well-defined conformational polymorphs of α-synuclein fibrils, that the activity of the Hsc70 disaggregase machinery is sensitive to differences in the amyloid conformation, confirming that fibril polymorphism directly affects interactions with the proteostasis network. Amyloid conformation influences not only how efficiently fibrils are cleared by the Hsc70 machinery but also the preferred pathway of disaggregation. We further show that, *in vitro*, the active processing of fibrils by the Hsc70 machinery inadvertently produces seeding competent species that further promote protein aggregation. Amyloid conformation thus is an important feature that can tilt the balance between beneficial or detrimental protein quality control activities in the context of disease.

Introduction

A hallmark of neurodegenerative diseases is the accumulation of amyloid-type aggregate deposits of signature proteins in patient brains. In synucleinopathies such as Parkinson's disease (PD), dementia with Lewy bodies (DLB) or multiple system atrophy (MSA), it is the intrinsically disordered protein α-synuclein (α-syn) that aggregates into such amyloid fibrils (Spillantini *et al*, 1997, 1998; Wakabayashi *et al*, 1998). Despite this common feature, the distribution and progression of pathological aggregate deposits differ strongly between diseases (Goedert, 2001; Barker & Williams-Gray, 2016; Holec & Woerman, 2021). It has been suggested that conformational differences in the amyloid structure adopted by α-syn, so called polymorphism, underlie the observed differences between synucleinopathies. This hypothesis is based on the observation that the amyloid structure found in MSA patients is distinct from that of Lewy Body diseases, DLB and PD (Schweighauser *et al*, 2020; Yang *et al*, 2022). The resulting differences in surface exposed residues can alter the interactions with cellular factors, leading to different modes and degrees of toxicity and spreading (Peng *et al*, 2018; Shahnawaz *et al*, 2020; Bousset *et al*, 2013; Van der Perren *et al*, 2020; Barker & Williams-Gray, 2016; Peelaerts *et al*, 2015; Hoppe *et al*, 2021).

As guardians of cellular proteostasis, molecular chaperones play an important role in preventing and reversing protein aggregation (Wentink *et al*, 2019; De Mattos *et al*, 2020; Hipp *et al*, 2019). The human constitutive 70kDa heat shock protein, Hsc70, and its co-chaperones, the J-domain protein DnaJB1 and the Hsp110 nucleotide exchange factor, Apg2, have been shown to efficiently resolubilise preformed amyloid fibrils of α-syn, the exon 1 of Huntingtin and different isoforms of tau (Scior *et al*, 2018; Duennwald *et al*, 2012; Nachman *et al*, 2020; Gao *et al*, 2015; Wentink & Rosenzweig, 2023). In this process, DnaJB1 identifies the amyloid fibrils as target via multivalent interactions with repeated low affinity binding sites in the flexible tails protruding from the amyloid fibrils and initiates the recruitment of Hsc70 (Wentink *et al*, 2020; Gao *et al*, 2015; Ayala Mariscal *et al*, 2022). Substrate recognition by DnaJB1 is important to efficiently cluster several Hsc70s on the fibril in functional cooperation with Apg2, generating an entropic pulling force that destabilises the fibril, leading to disaggregation (Faust *et al*, 2020; Wentink *et al*, 2020; Beton *et al*, 2022). An important binding site for DnaJB1 in α-syn is located in the C-terminal tail, while Hsc70 binding sites are present primarily in the N-terminus of the α-syn sequence (Redeker *et al*, 2012; Wentink *et al*, 2020; Nury *et al*, 2015; Burmann *et al*, 2020). In the context of different polymorph structures, these distinct binding sites might be buried or sterically occluded. This raises the question if different fibrillar α-syn polymorphs show differences in susceptibility to disaggregation by the chaperone machinery.

An Hsc70 mediated disaggregation mechanism based primarily on depolymerization, by monomer extraction from fibril ends, has been proposed (Beton *et al*, 2022; Franco *et al*, 2021; Schneider *et al*, 2021). However, the formation of smaller fibrillar fragments during the disaggregation of α-syn fibrils has also been documented (Beton *et al*, 2022; Gao *et al*, 2015). This mechanistic distinction is important as the extraction and accumulation of α-syn monomers is likely beneficial, whereas shorter fragments or oligomeric species produced as a result of fragmentation could constitute novel seeds for further amyloid aggregation and favour the propagation of α-syn pathology in a prion-like fashion (Marrero-Winkens *et al*, 2020; Tittelmeier *et al*, 2020; Woerman & Bartz, 2024). *In vivo* studies further highlight this ambiguity in the role of the Hsc70 chaperone machinery in synucleinopathy progression: both the overexpression and knockdown of the Hsp110 co-chaperone have been reported to protect against pathological α-syn aggregation and associated toxicity in animal models (Taguchi *et al*, 2019; Tittelmeier *et al*, 2022). Knockdown of the DnaJB1 co-chaperone in reporter cell lines similarly reduced the seeding capacity of some, but not all amyloid conformations of α-syn(Tittelmeier *et al*, 2022). Variation in chaperone mediated disaggregation kinetics and the resulting products among amyloid polymorphs may therefore contribute to the differences that are observed in disease progression and phenotypes in synucleinopathies (McCann *et al*, 2014; Hoppe *et al*, 2021; Tittelmeier *et al*, 2020).

In this study, we use *in vitro* aggregated fibrillar polymorphs of human WT α-syn to investigate how the Hsc70 disaggregase accommodates differences in amyloid structure, independent of amino acid sequence differences. These polymorphs are homogenous populations of structurally well-defined α-syn fibrils with distinct features such as a rigid or flexible α-syn N-termini and differences in the periodicity of twist, fibril length, width or stability (Gath *et al*, 2014; Bousset *et al*, 2013; Makky *et al*, 2016; Landureau *et al*, 2021). Such *in vitro* aggregated polymorphs are therefore a suitable model to experimentally explore how the disaggregation activity of the human Hsc70 chaperone system is affected by differences in amyloid structures on a biochemical level. We find that fibril conformation profoundly alters the ability of the Hsc70 chaperone machinery to recognize the substrate and consequently disaggregate α-syn amyloid fibrils. Polymorphs that were more resistant to chaperone action were more frequently fragmented during disaggregation, producing highly seeding competent species. The presence of a specific amyloid conformation can thus fundamentally alter the ability of the cell's quality control machinery to respond to this threat, which may have profound implications for the onset and progression of disease.

Results

α-synuclein fibrillar polymorphs show different susceptibility to disaggregation by the human Hsc70 chaperone machinery.

Recombinant monomeric α-syn protein was aggregated under various buffer conditions (see Material and Methods), resulting in five homogenous, structurally distinct amyloid polymorphs of full-length WT α-syn (FM, Ri, F65, F91 and XG) and one C-terminally truncated mutant (F110) (Fig. 1A and Extended Data Fig. 1A)(Gath *et al*, 2014; Gao *et al*, 2015; Bousset *et al*, 2013; Makky *et al*, 2016; Landureau *et al*, 2021). To test the susceptibility of the polymorphs to chaperone action, the preformed α-syn fibrils were incubated with the Hsc70 based disaggregase machinery, composed of the constitutively expressed Hsp70 family member Hsc70 (HSPA8), and two essential co-chaperones DnaJB1 and Apg2 (HSPA4/HSPH2). After 16 hours, the remaining insoluble fibrils were separated from re-solubilized α-syn by centrifugation (Fig. 1B, C). The sedimentation assay shows that the XG polymorph was efficiently disaggregated by the Hsc70 machinery in an ATP-dependent manner, with 40% of the total α-syn protein recovered in the soluble fraction. For the F65, FM and F91 polymorphs, 20-30% of α-syn protein was found in the supernatant, while Ri and F110 showed no release of soluble α-syn protein over the 16-hour incubation period.

We next compared the kinetics of disaggregation by time-resolved Thioflavin T (ThT)-based disaggregation assay (Fig. 1D, E). ThT is a fluorescent dye that shows enhanced fluorescence intensity upon interaction with β-sheet rich structures such as amyloid fibrils and can therefore be used to track the dissolution of amyloid fibrils (Biancalana & Koide, 2010). Since ThT shows differential reactivity to the polymorphs (Extended Data Fig. 1B), the fluorescence intensity during disaggregation was expressed as a ratio of non-disaggregated fibril intensity (-ATP) to facilitate comparison between the polymorphs. Based on ThT intensity, both XG and F65 polymorphs were efficiently disaggregated by the Hsc70 machinery within 16 hours, with ThT intensities reduced by 55% and 65% respectively. FM and F91 fibrils showed only moderate disaggregation, with a 15-25% reduction in ThT fluorescence. The reaction kinetics of the disaggregation of the F65 fibrils were noticeably faster in the first hour (1.5 fold) than that of the XG polymorph despite reaching a similar end point (Fig. 1D). The kinetics and endpoint of disaggregation of the FM and F91 polymorphs were comparable, and slower than both XG and F65. In contrast, for ribbons (Ri) and the C-terminal truncated F110 α-syn polymorphs the ThT-signal remained constant over 16 hours, indicating resistance to disaggregation by the human Hsc70 chaperone machinery.

Overall, the six α-syn polymorphs can thus broadly be divided into three categories: efficiently disaggregated (F65, XG), moderately disaggregated (FM, F91) and resistant to disaggregation by the

Hsc70 chaperone machinery (Ri, F110). Since all fibrillar polymorphs (except for F110) are composed of WT α-syn, the specific conformation of the fibrillar substrate thus directly affects the efficiency of chaperone mediated disaggregation.

Differences in polymorph structures perturb interactions with the chaperone machinery.

The differences observed in chaperone mediated disaggregation efficiencies may be explained by differences in the thermodynamic stability of the different fibril conformations, or the (in-)ability of chaperones to engage the substrate in a productive manner.

α-Syn fibrils exhibit differential stability at low temperature (Kim *et al*, 2008; Ikenoue *et al*, 2014; Bousset *et al*, 2013), where hydrophobic interactions are weakened, thus allowing to discriminate fibril conformations based on their thermodynamic stability. The relative stability of the polymorphs, based on their persistence at cold temperatures, serves as a broad discriminator between conformations that could or could not be disaggregated by the Hsc70 machinery (Extended data Fig. 2A-C), with the F110 and Ri conformations both most persistent at 4 °C and resistant to chaperone mediated disaggregation. However, resistance to cold temperatures did not readily explain the differences in disaggregation efficiency observed for the F65, XG, FM and F91 polymorphs.

A stronger correlation was observed between the affinity of the co-chaperone DnaJB1 for the different α-syn polymorphs, determined by fluorescence anisotropy, and the disaggregation efficiency, with the Ri conformation as notable outlier (r = -0.97, excluding Ri) (Fig. 2A, B). The affinity of the initial recognition of the amyloid substrate by DnaJB1 was found to differ up to 6-fold between α-syn fibril conformations, ranging from 200 nM to 1.5 μM. The efficiently disaggregated XG and F65 polymorphs clustered at the lower end of this range while DnaJB1 showed a reduced affinity for the more disaggregation resistant substrates FM, F91 and F110.

We next asked whether reduced recognition by DnaJB1 resulted in compromised recruitment of Hsc70 to the fibrils. Dissociation constants for DnaJB1-induced binding of Hsc70 to α-syn fibrils, determined by fluorescence anisotropy, spanned one order of magnitude, ranging from 140 nM for F65 to 1.5 μM for F110 (Fig. 2C, D). The correlation between Hsc70 binding affinity and disaggregation activity was however less pronounced than for DnaJB1 (r = -0.88, excluding Ri). While the extremes in affinity corresponded to the fibril polymorphs most efficiently disaggregated (F65) and resistant to disaggregation (F110), Hsc70 affinity alone could not explain the differences in disaggregation efficiency between the FM and XG polymorphs.

To test whether the differences in disaggregation efficiency observed reflect simply a lower chaperone occupancy of some of the polymorphs (due to lower chaperone affinities) under our experimental conditions, the ThT based disaggregation assay was repeated with 2-fold higher concentrations of chaperones. While increasing chaperone abundance accelerated the rates of the disaggregation reactions, it did not result in a lower endpoint ThT fluorescence for any of the α-syn fibrillar polymorphs (Extended Data Fig. 2D). Thus, the resistance to disaggregation of the F110 and Ri polymorphs, or the poor performance of the Hsc70 chaperone machinery on the FM and F91 polymorphs, cannot be surpassed simply by increased chaperone abundance. Rather, the reduced chaperone affinity for these conformations appears to reflect differences in the binding mode or positioning of the chaperones, resulting in chaperone machineries that are less conducive to disaggregation.

The three-dimensional structure of the α-syn amyloid polymorphs is thus likely to alter the accessibility of preferred chaperone binding sites in α-syn, resulting in differences in chaperone affinities and assemblies that are more, or less, efficient at generating the forces required for amyloid disaggregation (Wentink *et al*, 2020; De Los Rios *et al*, 2006; Goloubinoff & De Los Rios, 2007). In other instances, such as for the Ri conformation, it is likely that the inherent stability of the amyloid fibrils prevents disaggregation even when the Hsc70 machinery can successfully engage the substrate.

Polymorph structure influences the pathway of Hsc70 mediated amyloid disaggregation.

Recent studies have proposed different pathways of Hsc70 mediated disaggregation of α-syn fibrils (Schneider *et al*, 2021; Franco *et al*, 2021; Gao *et al*, 2015; Beton *et al*, 2022). Time resolved AFM and microfluidic diffusional sizing experiments indicated that disaggregation primarily proceeds via cooperative extraction of monomers from fibrils end, resulting in bursts of depolymerization. Instances of fibril fragmentation have however also been documented (Beton *et al*, 2022; Gao *et al*, 2015), although the relative frequency of these events remains uncharacterized. We hypothesize that these conflicting findings may be explained by differences in the amyloid structure of the fibrils studied. We therefore set out to characterize the reaction products formed during the disaggregation of the different α-syn amyloid conformations to document the preferred disaggregation pathway for each of the α-syn polymorphs.

Fluorescently labelled fibrils were incubated with the active chaperone machinery for 20 min, 2 hours or 16 hours and the reaction products analysed by sucrose density gradient centrifugation to determine the composition of products at different timepoints of the disaggregation reaction. Introduction of the fluorophore, post aggregation, did not change the morphology or efficiency of

disaggregation of the fibrils (Extended Data Fig. 3A-C), and labelling efficiencies were kept purposefully low (around 5% of α-syn monomers in the fibrils) to avoid fluorescence quenching in the fibrillar state (Extended Data Fig. 3D). Fluorescence intensity can thus be used as a quantitative read-out for the abundance of α-syn protein in the various fractions of the sucrose density gradient. Untreated fibrils of all polymorphs showed a sharp peak in fractions 12-20 (Extended Data Fig. 3E) corresponding to the highest sucrose concentration. Monomeric α-syn was instead found in fractions 0-2 (Extended Data Fig. 3F) at the top of the density gradient. Components of the chaperone machinery did not contribute to the fluorescence intensity signal (Extended Data Fig. 3G).

As negative control, fibrils were incubated with the chaperone machinery in the absence of ATP for 16h (Fig. 3A and Extended Data Fig. 3H, "No Disagg"). These non-disaggregated fibrils were found in the bottom fractions of the density gradient corresponding to large, unprocessed fibrillar material. After 20 min incubation with the active disaggregation machinery (with ATP), the polymorph F65 showed a major shift of up to 60% of α-syn fluorescence into fractions 3-10. As fractions 0-2 were found to correspond to the α-syn monomer, fraction 3-10 contain a heterogenous range of species of intermediate oligomeric state, in molecular weight distinct from fibrils and α-syn monomer. This peak thus likely corresponds to shortened fibrils, smaller fibril fragments or oligomers produced during Hsc70 mediated disaggregation. The fluorescence signal in fractions 3-10 is reduced with increasing reaction times, with a corresponding increase in fluorescence intensity in the monomer fractions 0-2 (Fig. 3A), indicating a conversion of the shortened fibrils/oligomers to monomers as the disaggregation reaction proceeds.

The polymorphs FM, XG and F91 display similar trends, with a decrease in fibril peak intensity concomitant with a rapid conversion into shorter α-syn fibrils/oligomers and monomers over time (Fig. 3A, Extended Data Fig. 3H). In contrast, the sucrose density gradient results for Ribbons (Ri) and the C-terminal truncated mutant F110 presented no changes in size distribution over 16 hours with all fluorescence intensity found in fraction 12-20, corresponding to unprocessed fibrils (Fig. 3A, Extended Data Fig. 3H). These polymorphs are thus indeed not processed by the Hsc70 chaperone machinery.

The sucrose density gradient results for the FM and F91 fibrils diverge from the ThT assays which reported only limited disaggregation activity. Quantification of the relative abundance of the monomer (fraction 0-2), oligomers and shortened fibrils (3-10) and fibrils (12-20) fractions for the FM and F91 polymorphs at the different timepoints (Fig. 3B) indicate that while fluorescence intensity in the fibrillar fractions rapidly decreased and stabilized from 20 min onwards around 55% and 20% of the starting fluorescence intensities respectively, α-syn monomers accumulate very slowly and are absent

(<5%) at 20 min. The main products of chaperone mediated disaggregation of the FM and F91 polymorphs, found in fractions 3-10, are thus likely to be fibril fragments, produced as the result of fibril fragmentation. Such fragments would retain ThT binding capacity and sediment upon centrifugation, explaining the apparent poor disaggregation efficiencies detected by previous experiments. The Hsc70 machinery can thus in fact process the FM and F91 α-syn fibrillar polymorphs efficiently but relies on a disaggregation pathway dominated by fibril fragmentation.

In contrast, the distribution of reaction products of the F65 polymorph are consistent with a disaggregation mechanism driven primarily by depolymerization of monomers from fibril ends (Franco *et al*, 2021; Schneider *et al*, 2021; Gao *et al*, 2015; Beton *et al*, 2022), with a gradual reduction in the fibrillar fraction over time and the appearance of monomers at early timepoints (Fig. 3B). As a consequence, the oligomer/fragments species are less abundant and more broadly distributed, with the average size shrinking as a function of time during the disaggregation of F65 as reflected by their position in the gradient (Fig. 3A). The XG fibrils display an intermediate behaviour, with rapid processing of the initial fibril material into smaller oligomeric species followed by relatively efficient conversion to monomers (Fig. 3B), suggesting a disaggregation pathway that combines depolymerisation and fragmentation.

Fibril conformation can thus alter the preferred pathway of amyloid disaggregation by the Hsc70 machinery, with depolymerization dominating the disaggregation of F65, and fragmentation contributing significantly to the disaggregation of FM and F91. We conclude from our results that fibril fragments and/or oligomers accumulate to different extent during the chaperone mediated disaggregation of distinct α-syn fibrillar polymorphs.

Disaggregation of α-synuclein fibrils produces seeding competent species in vitro.

Pathological protein aggregates associated with neurodegenerative disease have been hypothesized to propagate in a prion-like fashion, where initial amyloid seeds can serve as conformational template to promote further aggregation (Tittelmeier *et al*, 2020; Marrero-Winkens *et al*, 2020; Braak *et al*, 2003; Jucker & Walker, 2018). The differential accumulation of oligomer/fragment species during chaperone mediated disaggregation among α-syn polymorphs thus may alter their ability to propagate and spread from cell to cell in a disease context.

To evaluate the potential role of chaperone mediated disaggregation in the prion-like amplification of α-syn seeds, the seeding capacity of the disaggregation reaction products was characterized for the F65 and FM polymorphs as representative examples of amyloid conformations where disaggregation

occurs primarily by depolymerization or where fragmentation is prevalent, respectively. The seeded aggregation of α-syn monomers was monitored *in vitro* by ThT fluorescence (Fig. 4A and B). The untreated fibrils seeded the aggregation of α-syn monomers efficiently. Incubation with an inactive chaperone machinery ("No disagg") resulted in a factor 2 decrease in seeding rates, consistent with an expected prevention of aggregation activity of the Hsc70 machinery (De Mattos *et al*, 2020). The prior disaggregation of F65 and FM fibrils for 16 hours did not reduce the seeding capacity further (Fig. 4A and B). This is surprising as the ATP driven disaggregation activity of Hsc70 processes 75% and 40% of the starting material, respectively, over 16 hours (Fig. 3B) and a corresponding drop in the seeding capacity might be expected if the residual unprocessed fibrils were the only source of seeds in these reaction mixtures. Disaggregation of both the FM and F65 polymorphs thus produces a novel seeding competent species.

To identify the novel seeding competent species in the reaction mixtures, the total disaggregation reactions were fractionated by centrifugation (Fig. 4C). Residual unprocessed fibrillar material was depleted from the disaggregation products by low-speed centrifugation (15 min at 3,600g). Higher centrifugation speeds (30 min at 435,630g) additionally separated monomers from smaller fragments/oligomers as confirmed by electron microscopy and sucrose density gradients (Fig. 4D and Extended Data Fig. 4A-C). For both polymorphs, the supernatant of the low-speed centrifugation step retained a large fraction of the seeding capacity of the total disaggregation mixture. The high-speed centrifugation sample was however seeding incompetent (Fig. 4E, F). In contrast, the fractionation of fibrils treated with the inactive chaperone machinery, showed a total depletion of seeding capacity even after the first low speed centrifugation step (Fig. 4G and H). The new seeding competent species created through the disaggregation of α-syn fibrils thus likely comprise smaller fibril fragments or oligomers that retains features of the amyloid conformation.

The initial aggregation rate of α-syn monomers seeded with the F65 low-speed centrifugation fraction is reduced by only 25% compared to the total reaction mixture (Fig. 4E, F), consistent with 75% of the starting material having been processed to smaller fibril or oligomers now found in this soluble fraction (Fig. 3B). This fraction contains a mixture of released monomers and fibril fragments primarily the result of fibril shortening by depolymerisation. Disaggregation by a pathway where depolymerisation is dominant thus results in a lower total mass of fibrils overtime, but broadly preserves the total number of fibril ends in the sample that can serve as template for amyloid fibril growth when disaggregation does not go to completion.

In contrast, the same fraction of fragments/oligomers of the FM polymorph, containing only 40% of the starting fibrillar material (Fig. 3B), accounted for 60% of the seeding capacity of the total reaction mixture (Fig. 4E, F). This suggests that the newly formed products are per monomer equivalent more seeding competent than the original starting material. This is consistent with our observation that FM fibrils are sensitive to fragmentation during disaggregation, which would result in a growing number of smaller fibrils, each capable of templating further protein aggregation. This, despite an overall decrease in total aggregate mass by Hsc70 mediated disaggregation.

Despite these differences, both α-syn polymorph samples retained a large fraction of their *in vitro* seeding capacity after 16 hours of disaggregation, suggesting that unless fibrils are fully dissolved to monomers, Hsc70 mediated disaggregation may have limited protective function against further protein aggregation. Nevertheless, the anti-aggregation activity of the Hsc70 machinery observed in the reactions without ATP ("No disagg") compared to the untreated fibrils ("Fibrils") in Fig. 4A, B dominates these *in vitro* seeding reactions, indicating a net protective effect of the presence of the Hsc70 machinery on both α-syn polymorphs *in vitro*.

Disaggregation reaction products trigger intracellular aggregation of α-syn in human cells.

We next assessed the seeding capacity of the Hsc70 machinery-derived α-syn species from the different polymorphs in a cellular context. To this end, we used a well-established HEK293 biosensor cell line (Sanders *et al*, 2014; Tittelmeier *et al*, 2022) that stably expresses aggregation prone A53T mutant α-syn, C-terminally fused to yellow fluorescent protein (α-syn A53T-YFP) (Fig. 5A). Before exposure to recombinant α-syn fibrils, the α-syn A53T-YFP reporter exhibited diffuse cytosolic fluorescence (Fig. 5B, panel "untreated"). Once exposed to the α-syn polymorphs, we observed the accumulation of fluorescent α-syn A53T-YFP foci within the cells, reflecting intracellular aggregation of the reporter seeded by inoculated fibrils (Fig. 5A, B). To reduce potential differences in cell surface binding and uptake efficiency between structurally distinct α-syn fibrillar polymorphs, fibrils were introduced into the cytosol with lipofectamine. Except for the Ri conformation, all α-syn fibrillar polymorphs induced intracellular aggregation of α-syn in up to 15% of cells (Fig. 5A, B and Extended Data Fig. 5A, B).

The seeding capacity of the FM, F65, F91 and XG polymorphs is reduced by 2- to 4-fold after incubation with the chaperone machinery in the absence of ATP ("No Disaggregation", Fig. 5B, C and Extended Data Fig. 5A, B). In contrast, the seeding capacity of the F110 polymorph was unaltered by pre-incubation with the Hsc70 chaperone machinery ("No Disaggregation", Extended Data Fig. 5A, B). We hypothesized that the observed prevention of aggregation activity could be attributed to a direct

interaction of chaperones with the fibrils. Incubation with individual components of the Hsc70 chaperone machinery identified DNAJB1 as the key chaperone responsible for reducing the seeding capacity of XG α-syn fibrils to 30% of the untreated fibrils (Extended Data Fig. 6). In contrast, no combination of chaperones affected the seeding capacity of the F110 polymorph, consistent with the reduced affinity of the Hsc70 chaperone machinery for this polymorph (Extended Data Fig. 6A and Fig. 2).

Incubation of α-syn fibrillar polymorphs sensitive to disaggregation with the active chaperone machinery increased their overall seeding capacity by 3-4 fold compared to their seeding propensity upon incubation with the chaperones in the absence of ATP ("Disaggregation" vs "No Disaggregation", Fig. 5B, C). Thus, despite an overall decrease in amyloid content ranging from 40-80% after disaggregation in all of these reactions (Fig. 3B), the resulting material approximates the seeding capacity of the fibrils prior to exposure to chaperones. This seeding ability could again be attributed primarily to small oligomers/fragments produced during disaggregation, rather than the residual unprocessed fibrils, based on fractionation of monomer, oligomer and fibril fractions by centrifugation (Fig. 4C). The cellular context thus negates in large part the protective effects of the chaperone machinery (as observed in the "No disaggregation" samples, Fig. 5) while amplifying the potential threat associated with the production of fibrillar fragments/oligomers during chaperone mediated disaggregation as compared to *in vitro* experiments.

Discussion

In this study we show that conformationally distinct fibrillar polymorphs prepared from recombinant human α-syn protein, exhibit differential susceptibility to disaggregation by the human Hsc70 chaperone machinery. High thermodynamic stability of the specific conformation, as deduced from a lack of depolymerisation at low temperatures, is associated with a complete resistance to chaperone mediated disaggregation under the tested conditions suggests there is a thermodynamic limit to the ability of the chaperone machinery to disaggregation amyloid fibrils. Furthermore, chaperone affinity correlates well with disaggregation efficiency but furthermore appears to determine the dominant pathway of disaggregation, with high affinity substrates such as the F65 fibrils being mainly disaggregated via depolymerization into monomeric α-syn, while more fragmentation occurred with less ideal target conformations such as the FM and F91 polymorphs (Fig. 6A).

The observed differences in chaperone affinity likely reflect the accessibility and geometry of important chaperone binding sites in the N- and C-terminus of α-syn (Fig. 6B)(Redeker *et al*, 2012; Wentink *et al*, 2020; Burmann *et al*, 2020; Nury *et al*, 2015). DnaJB1 is seemingly most sensitive to

these differences, consistent with the report that its affinity for the aggregated state of α-syn is driven by avidity effects (Wentink et al, 2020), which would be affected by distance or orientation of proximal binding sites. Little structural information is available about this region as it remains highly unstructured in all fibrillar states. The differences in DnaJB1 affinity for the α-syn polymorphs are however consistent with those of a C-terminal specific antibody 10D2 (Landureau *et al*, 2021) which binds the Ri conformation more strongly than the FM and F91 fibrils, suggesting reduced accessibility or potential for multivalent binding in these conformations.

Similarly, the subsequent recruitment of Hsc70 is likely to be affected by (1) the positioning of DnaJB1 and (2) the degree of structure of the α-syn N-terminus where important Hsc70 binding sites reside. Key variations in the degree of structure in this region were described for the different studied α-syn polymorphs (Fig. 6B)(Landureau *et al*, 2021). For example, in the Ri polymorph the N-terminus is highly ordered, potentially altering the binding mode of Hsc70 and thus its ability to assemble into disaggregation competent complexes.

The different sensitivities of α-syn polymorphs to disaggregation has potentially important implications for disease progression. Disaggregation pathways with higher fragmentation rates would lead to the creation of shorter fibrils, which we show are coupled to a higher *in vitro* seeding capacity. Fibril conformations that predominate in disease may therefore be those that are most sensitive to fragmentation, boosting their amplification and propagation. Furthermore, brain cells where chaperone mediated disaggregation is most active, may be most susceptible to pathology onset and progression when compared to neighbouring cells that survive.

C-terminal proteolysis of α-syn is frequently observed in Lewy-bodies (Zhang *et al*, 2017; Li *et al*, 2005; Liu *et al*, 2005). We could demonstrate that a missing C-terminus leads to a resistance to disaggregation, most likely because important chaperone binding sites are located in the flexible C-terminus of the α-syn fibrils (Wentink *et al*, 2020; Redeker *et al*, 2012). This posttranslational modification might thus transfer the protein aggregate into a state that is resistant to clearance by chaperones and result in its accumulation in patient brains. In the context of our observation that disaggregation significantly increased the intracellular seeding capacity of α-syn fibrils, this induced resistance to disaggregation may in fact inhibit further aggregate propagation. This posttranslational modification could therefore be a protective mechanism against prion-like propagation of the disease phenotype.

Our study also highlights the emergent properties of the complex cellular environment, with seeding capacity of disaggregation products generated *in vitro* (Fig. 5) strongly amplified in cell-based assays compared to *in vitro* experiments (Fig. 4). As a counterpoint, the effective coupling of disaggregation pathways to refolding or degradation pathways within the cellular context may result in synergies in the intracellular disaggregation of α-syn fibrils that were not explored in this study. For instance, in case of tau fibrils, the Hsc70 machinery can act downstream of the VCP/p97 chaperone machinery. The AAA+ ATPase VCP/p97 pre-processes ubiquitinated tau fibrils by fragmentation but relies on Hsc70 action to fully dissolve existing tau aggregates (Saha *et al*, 2023). Such synergies may alleviate some of the potential dangers associated by fragment production during disaggregation (Nachman *et al*, 2020). It will thus be important to investigate the balance between protective and harmful chaperone activities within the cellular context.

Taken together, the cellular chaperone machinery may differently affect the formation and clearance of α-syn amyloid fibrils in different synucleinopathies, depending on the predominant α-syn polymorph. This model makes it challenging to design a universal approach to exploiting chaperones for therapeutic applications. Nevertheless, these findings highlight the importance of considering conformational diversity when investigating the molecular basis of pathological protein aggregation and possible future therapeutics that intervene in the process.

Material and Methods

Protein expression and purification

Chaperone proteins, Hsc70, DnaJB1, Apg2, and mutants (DnaJB1-G194C, Hsc70-C267A-C574A-C603A-T111C) were purified as previous described (Nillegoda *et al*, 2015). Briefly, proteins were expressed as His_6-Smt3 (H6-sumo) fusion proteins in *E. coli* BL21 Rosetta cells, followed by nickel affinity purification (Ni-IDA, Macherey-Nagel) after lysis. Tag-cleavage by ULP1 protease overnight and a second, reverse nickel affinity purification was carried out to remove the tag.

Wild-type α-synuclein was recombinantly expressed from a pT7-7 or pET14b expression vector as untagged protein in E. coli (DE3) Gold and purified as previously described (Hoyer *et al*, 2002; Ghee *et al*, 2005).

Fibril preparation

Purified α-syn monomers were aggregated in the corresponding buffer under continuous shaking for 7 days at 37 °C (**Buffer Compositions:** XG- 50 mM $NaHPO_4$, 100 mM NaCl, pH 7.3, 1000 rpm; FM - 50 mM Tris-HCl 150 mM, KCl, pH 7.5, 600 rpm; Ri - 5 mM Tris-HCl, pH 7.5, 600 rpm, F65 - 20 mM MES, 150 mM NaCl, pH 6.5, 600 rpm; F91 - 200 mM KPO_4, pH 9.1, 600 rpm). The C-terminal truncated α-syn (aa 1-110) was aggregated in 50 mM Tris-HCl 150 mM KCl, pH 7.5, 600 rpm (Bousset *et al*, 2013; Makky *et al*, 2016). Fibril concentrations are expressed as the concentration of their constituent α-syn monomers.

For sucrose density gradient experiments, pre-aggregated fibrils of the different polymorphs (100 µM) were incubated with AF-555 Succinimidylester (15 µM) in 50 mM $NaHPO_4$, 100 mM NaCl buffer at pH 7.6 for 4 h at RT. Free fluorophore was removed by two times 30 min centrifugation at 435,630 g. Labelling efficiency was determined to be 5-8% by absorbance after denaturing of the fibrils in 5M GnHCl. Quenching due to high fluorophore density was ruled out by confirming the absence of an increase of fluorescence signal upon denaturing of the fibrils in 4M GnHCl measured in CLARIOstar plate-reader (BMG LABTECH, 555nm). 60% AF-555-labeled XG fibrils and AF-555 labelled α-syn monomers are used as a control for fluorophore quenching positive and negative samples respectively.

Electron microscopy

Electron microscopy images were used to visualise differences in fibril polymorphs and samples. Immediately before sample application, grids (Copper Grids, 300 square, 3.05 mm coated with a carbon film) were glow discarded for 20 sec with 80 mA. Samples were applied at a fibril concentration of 2 µM. Grids were placed on a 10 µL sample drop for 1 min, followed by directly transferring the grid into 3-5 wash steps of 1 mL H_2O drops. Last, the grids were placed in 1% uranyl acetate and incubated

for 1 min. The excess of uranyl acetate was removed with Whatman paper. Grids were imaged in a transmission electron microscope ZEISS 910 at 80 kV (Carl Zeiss, Oberkochen, Germany) using a slow scan CCD camera (Albert Tröndle (TRS), Moorenweis, Germany).

Fibrillar polymorphs fingerprinting by limited proteolysis

As structurally distinct fibrillar α-syn polymorphs exhibit characteristic proteolytic profiles, we subjected each polymorph (1.4 mg/mL equivalent monomer concentration) in PBS at 37 °C to Proteinase K (3.8 µg/mL) (Roche) treatment. Aliquots (10 µL) were removed at different time intervals following addition of the protease (0, 1, 5, 15, 30, and 60 min) and transferred into Eppendorf tubes containing PMSF (1 µL, 100 mM in ethanol). The samples where dried using speed vacuum and further solubilized by addition of pure HFIP (Hexafluoroisopropanol, 30 µL). After overnight incubation at RT, HFIP was evaporated, the samples were resuspended in Laemmli buffer, heated 10 min at 80 °C, and processed for Tris-Glycine SDS-PAGE (15%) analysis.

Thioflavin T (ThT) binding

ThT binding reactivity was analysed to show structural differences between the different polymorphs. 2 µM fibrils were incubated with 30 µM ThT in 50 mM HEPES-KOH (pH 7.5), 50 mM KCl, 5 mM $MgCl_2$, 2 mM DTT for 30 min. Fluorescence intensity was measured in a Biotech Omega plate reader at RT (excitation: 440 nm, emission: 480 nm).

ThT Disaggregation assay

The fibril amount in a disaggregation reaction was monitored over time by the ThT signal of the fibrils. 2 µM fibrils were incubated with 4 µM Hsc70, 2 µM DnaJB1, and 0.2 µM Apg2 in reaction buffer (50 mM HEPES-KOH (pH 7.5), 50 mM KCl, 5 mM $MgCl_2$, 2 mM DTT) and 30 µM ThT in the presence of 2 mM ATP and ATP regeneration system (3 mM PEP and 20 ng μl^{-1} pyruvate kinase), as described (Wentink *et al*, 2020). The samples were incubated for 16 h in 50 µL reaction volume at 30 °C in a BMG Labtech FLUOstar Omega plate reader. Measurements were collected at excitation wavelength: 440 nm and emission wavelength: 480 nm. Background measurements of buffer and inactive chaperone machinery (in the absence of ATP and ATP regeneration) were subtracted and all samples were normalized to the fluorescence intensity at timepoint t=0. Experiments were carried out in three biological replicates of different fibril batches. Each biological replicate datapoint is an average of at least 2 technical replicates.

The 2-fold increased chaperone concentration experiments were performed with 2 µM fibrils and 8 µM Hsc70, 4 µM DnaJB1 and 0.4 µM Apg2, 2mM ATP and ATP regeneration system.

Supernatant pellet assay

To confirm the ThT disaggregation results, disaggregation of fibrils was determined by analysis of the supernatant and pellet fraction before and after incubation with the active chaperone machinery. Fibrils or labelled fibrils (2 µM) were centrifuged for 15 min at 3,600 g after incubation with chaperones (4 µM Hsc70, 2 µM DnaJB1, and 0.2 µM Apg2) in the presence or absence of ATP (2 mM) and ATP-regeneration system for 16 h in reaction buffer. Supernatant and pellet were separated and run on an SDS page gel (Bis-Tris gel 4-20%) followed by immunoblotting (primary antibodies: α-syn (SNAC) monoclonal mouse IgG (Sc-12767), α-syn (SNAC) (61-95) monoclonal mouse IgG (SM6028), secondary antibody: Alkaline phosphatase coupled anti-mouse-IgG (H+L) (horse)). Membranes were imaged with a LAS-4000 instrument and quantification performed in ImageJ. The released material found in the supernatant was expressed as the fraction of the sum of the pellet and supernatant band intensities.

Cold denaturation

To visualise differences in chemical stability the different fibrillar polymorphs were incubated on ice. At the indicated time in hours, an aliquot (50 µL) was removed and spun for 30 min at 50,000 g. The supernatant was recovered, denatured with Laemmli buffer and analysed by PAGE (15% polyacrylamide), stained with Coomassie blue and imaged (ChemiDoc MP (BioRad)). To determine the proportion of α-syn in the supernatant, the total amount of α-syn is run in parallel. The band intensities were quantified on the ChemiDoc MP (BioRad) used to image the gels and analysed with ImageLab (version 5.2.1).

Fluorophore labelling of chaperones

Chaperones mutants (DnaJB1-G194C, Hsc70-C267A-C574A-C603A-T111C) were labelled on free reactive cysteines with Alexa-488 or 594 C5 maleimide. Buffer was exchanged with D SpinTrap G25 columns into 25 mM HEPES, 150 mM KCl, 5 mM MgCl and 5% glycerol and chaperones incubated for 30 min at 30 °C in the presence of 100 µM TCEP. ATP was added to a final concentration of 5 mM for reactions containing Hsc70 to prevent the labelling of the remaining native cysteine residue C17 in the ATP binding pocket. An 8-fold molar excess fluorophore label was added, and proteins incubated for 1h at RT. Excess fluorophore was removed by two subsequent D SpinTrap G25 column runs. Labelling efficiency was 90% or higher, based on absorbance measurements of the fluorophore and protein concentrations (Extinction coefficient: Hsc70 33600 L/mol*cm, DnaJB1 19033 L/mol*cm).

Steady-state anisotropy

To determine chaperone binding to the different fibrils, equilibrium binding was measured by fluorescence anisotropy of labelled DnaJB1-G194C or Hsc70-C267A-C574A-C603A-T111C to fibrils after

incubation for 3.5 h at 25 °C (buffer: 50 mM HEPES-KOH (pH 7.5), 50 mM KCl, 5 mM $MgCl_2$, 2 mM DTT), as previous described(Wentink *et al*, 2020). Fibril binding data of 100 nM AF-594-labeled DnaJB1 mutant G194C or 100 nM AF-488-labeled Hsc70 mutant T111C in the presence of 50 nM DnaJB1 were acquired in CLARIOstar plate-reader (BMG LABTECH, for AF-488-labeled protein: excitation: 482 nm, emission: 530 nm, dichroic filter: 504 nm or for AF-594-labeled protein excitation: 590 nm, emission: 675 nm, dichroic filter: 639 nm). Dissociation constants were determined in GraphPad Prism, by fitting the data to a model describing equilibrium binding by non-linear regression.

Sucrose density gradient experiments

Reaction products were separated by sucrose gradient centrifugation. A disaggregation reaction with labelled fibrils (2 µM; 4 µM Hsc70, 2 µM DnaJB1, and 0.2 µM Apg2) was carried out for 20 min, 2 h, and 16 h in the presence of ATP (2 mM) and ATP-regeneration system in reaction buffer at 30 °C. After completion of the reaction time, ATP was depleted with alkaline phosphates (0.1 U/µL, Roche). As negative control alkaline phosphatase was added from timepoint 0 and incubated for the maximal reaction time of 16 h. Furthermore, samples of untreated fibrils, chaperones only, and monomers were analysed. Samples were applied on a sucrose gradient (SW40, 10-85% sucrose) and centrifuged 30 min at 3,500 rpm (217,290 g). Gradients were fractionated by Biocomp Piston Gradient Fractionator™ coupled with a Triax™ flow cell (mCherry). For quantification of monomer (fractions 0-2), small fragments/oligomers (fractions 3-10), and fibrils (fractions 12-20) fluorescence intensity values of specific fractions were summed up and divided by total fluorescence intensity across the gradient. All calculations were performed on the raw data, plotted data has been smoothed in Graphpad Prism as a rolling average of 10 datapoints.

Differential centrifugation of disaggregation reaction products

The products of chaperone mediated disaggregation were fractionated by distinct centrifugation steps, as shown in Fig. 4C. A disaggregation reaction (1:2:1:0.1 fibrils/Hsc70/DnaJB1/Apg2 in 50 mM HEPES-KOH (pH 7.5), 50 mM KCl, 5 mM $MgCl_2$, 2 mM DTT, 2 mM ATP, and ATP regeneration system) was incubated for 16 h at 30 °C. After completion of the reaction time, ATP was depleted with alkaline phosphates (0.1 U/µL, Roche) to quench the reaction. As negative control alkaline phosphatase was added from timepoint 0 h and incubated for 16 h ("No disaggregation").

The total sample was divided into three samples. One was not centrifuged to reflect the total disaggregation reaction. The oligomer/small fragment sample was prepared collecting the supernatant after centrifugation at 3,600g for 15 min to deplete large unprocessed fibrils from the mixture. The monomer sample was depleted of fibrils and oligomers and fibril fragments by centrifugation at 435,630 g for 30 min.

In-vitro seeding assay

The aggregation behaviour of the reaction products was first analysed in-vitro. Aggregation of 20 µM α-syn monomer was induced with 10% seeds in the presence of 30 µM ThT and 0.05% NaN_2. Seeds concentrations were expressed as α-syn monomer concentrations. Untreated fibrils, fibrils incubated with chaperones (ATP depletion with alkaline phosphates (0.1 U/µL, Roche) at timepoint 0 (No disaggregation) or timepoint 16 h (Disaggregation)), and disaggregation reactions fractionated by centrifugation were used as seeds. For the disaggregation reactions, 10 µM fibrils were incubated with 20 µM Hsc70, 10 µM DnaJB1, and 1 µM Apg2 in reaction buffer (50 mM HEPES-KOH (pH 7.5), 50 mM KCl, 5 mM $MgCl_2$, 2 mM DTT) with 2 mM ATP.

The seeded aggregation reactions were monitored under continuous shaking (1000 rpm) for 80 h at 37 °C in a 96-well plate in a Biotech Omega plate reader. Fluorescence intensity measurements were collected at wavelengths excitation: 440 nm, emission: 480 nm. The Initial velocity was calculated by fitting a linear regression over the first 20 min of seeding.

Seeding assay in cell culture

To confirm in-vitro seeding experiments, seeding of the samples were also tested in cells. Cell culture experiments were performed as previously described (Tittelmeier *et al*, 2022). Cells were cultured in DMEM (high glucose, GlutaMAX Supplement, pyruvate, 10% FBS, 1x Penicillin-Streptomycin) at 37 °C and 5% CO_2. The HEK293T cell line expressing α-synA53T-YFP was a gift by Marc Diamond, University of Southwestern Texas.

Disaggregation reactions were performed as described under the header In-vitro seeding assay. Cells were seeded with the resulting disaggregation reaction mixtures or fractionated reaction products, depleted of ATP with alkaline phosphates (0.1 U/µL, Roche) at timepoint 0 (No disaggregation) or timepoint 16 h (Disaggregation)) to quench ongoing disaggregation reactions.

The concentration of reaction mixtures or reaction products was adjusted to 2 µM α-syn monomer concentration in Opti-MEM Reduced Serum Medium, GlutaMAX Supplement (Gibco). Pre-incubated Lipofectamine2000 with Opti-MEM (1:20 dilution, 5 min) was added to samples (1:1) for a second incubation step of 20 min. The mixture was then added to cells seeded on coverslips coated with Poly-L lysine (Invitrogen) in 24-well plates in a final concentration of 100 nM. After 48 h cells were fixed (4% PFA in PBS, 10 min), washed with PBS (3x), and mounted for imaging. Cells were imaged with a confocal microscope Leica TCS SP8 STED 3X microscope (Leica Microsystem, Germany). Images were processed with ImageJ and FIJI was used to manually quantify cells and cells with foci. Ten images per condition with 30-100 cells per images were analysed. The percentage of cells with foci was calculated and significance of all changes were calculated by nonparametric Two-Way ANOVA with pairwise comparisons of estimated marginal means with Tukey correction for multiple comparisons.

Data availability:

This study includes no data deposited in external repositories. All data supporting the findings of this study are available within the paper and its supplemental material.

Acknowledgements

The authors would like to thank the Deutsches Krebsforschungszentrum (DKFZ) Electron Microscopy facility and Ania Alik for technical support. We are indebted to A. Mogk and M. Mayer for valuable discussions throughout the project. The authors further acknowledge M. Diamond for providing the HEK293 α-SynA53T-YFP biosensor cell line. This is an EU Joint Programme – Neurodegenerative Disease Research (JPND) project (PROTEST-70). This project is supported through the following funding organizations under the aegis of JPND - www.jpnd.eu: France, Agence National de la Recherche (ANR, ANR-17-JPCD-0005-01 to RM); Germany, Bundesministerium für Bildung und Forschung (01ED1807A to BB and 01ED1807B to CNK). This research has further been funded by the Deutsche Forschungsgemeinschaft (DFG, German Research Foundation) – project number 504257241 to BB, a standard grant from the Alzheimer Forschungs Initiative to BB, by the Dutch Research Council (NWO, Vidi grant number VI.Vidi.223.172) to ASW and support from France Parkinson and EraPerMed DEEPEN-iRBD project (ANR-22-PERM-0006) to RM. AKB thanks the Novo Nordisk Foundation (grant number NNFSA170028392) and the Lundbeck Foundation (grant number R366-2021-169) for funding. SJ acknowledges the HBIGS graduate school for support.

Disclosure and competing interest statement.

The authors declare that they have no conflict of interest.

Author Contributions

Conceptualization S.J., A.K.B., R.M., C.N., B.B., A.S.W.

Data curation S.J., J.T., R.M.

Formal Analysis S.J., A.S.W.

Funding acquisition R.M., C.N., B.B., A.S.W.

Investigation S.J., J.T., T.L.D., R.M.

Methodology S.J.

Project administration R.M., C.N., B.B., A.S.W.

Resources T.L.D., T.B., V.R.

Supervision R.M., C.N., B.B., A.S.W.

Visualization S.J.

Writing – original draft S.J., A.S.W.

Writing – review & editing S.J., J.T., T.L.D., A.K.B., C.N., R.M., B.B., A.S.W.

References

Ayala Mariscal SM, Pigazzini ML, Richter Y, Özel M, Grothaus IL, Protze J, Ziege K, Kulke M, ElBediwi M, Vermaas J V., *et al* (2022) Identification of a HTT-specific binding motif in DNAJB1 essential for suppression and disaggregation of HTT. *Nat Commun* 13

Barker RA & Williams-Gray CH (2016) The spectrum of clinical features seen with alpha synuclein pathology. *Neuropathol Appl Neurobiol* 42: 6–19

Beton JG, Monistrol J, Wentink A, Johnston EC, Roberts AJ, Bukau BG, Hoogenboom BW & Saibil HR (2022) Cooperative amyloid fibre binding and disassembly by the Hsp70 disaggregase. *EMBO J* 41: e110410

Biancalana M & Koide S (2010) Molecular mechanism of Thioflavin-T binding to amyloid fibrils. *Biochim Biophys Acta Proteins Proteom* 1804: 1405–1412

Bousset L, Pieri L, Ruiz-Arlandis G, Gath J, Jensen PH, Habenstein B, Madiona K, Olieric V, Bockmann A, Meier BH, *et al* (2013) Structural and functional characterization of two alpha-synuclein strains. *Nat Commun* 4: 2575

Braak H, Tredici K Del, Rüb U, de Vos RAI, Jansen Steur ENH & Braak E (2003) Staging of brain pathology related to sporadic Parkinson's disease. *Neurobiol Aging* 24: 197–211

Burmann BM, Gerez JA, Matečko-Burmann I, Campioni S, Kumari P, Ghosh D, Mazur A, Aspholm EE, Šulskis D, Wawrzyniuk M, *et al* (2020) Regulation of α-synuclein by chaperones in mammalian cells. *Nature* 577: 127–132

Duennwald ML, Echeverria AL & Shorter J (2012) Small heat shock proteins potentiate amyloid dissolution by protein disaggregases from yeast and humans. *PLoS Biol* 10

Faust O, Abayev-Avraham M, Wentink AS, Maurer M, Nillegoda NB, London N, Bukau B & Rosenzweig R (2020) HSP40 proteins use class-specific regulation to drive HSP70 functional diversity. *Nature* 587: 489–494

Franco A, Gracia P, Colom A, Camino JD, Fernández-Higuero JÁ, Orozco N, Dulebo A, Saiz L, Cremades N, Vilar JMG, *et al* (2021) All-or-none amyloid disassembly via chaperone-triggered fibril unzipping favors clearance of α-synuclein toxic species. *Proceedings of the National Academy of Sciences* 118: e2105548118

Gao X, Carroni M, Nussbaum-Krammer C, Mogk A, Nillegoda NB, Szlachcic A, Guilbride DL, Saibil HR, Mayer MP & Bukau B (2015) Human Hsp70 Disaggregase Reverses Parkinson's-Linked alpha-Synuclein Amyloid Fibrils. *Mol Cell* 59: 781–793

Gath J, Bousset L, Habenstein B, Melki R, Böckmann A & Meier BH (2014) Unlike twins: An NMR comparison of two α-synuclein polymorphs featuring different toxicity. *PLoS One* 9: 1–11

Ghee M, Melki R, Michot N & Mallet J (2005) PA700, the regulatory complex of the 26S proteasome, interferes with α-synuclein assembly. *FEBS Journal* 272: 4023–4033

Goedert M (2001) Alpha-Synuclein and Neurodegenerative Diseases. *Nat Rev Neurosci* 2: 492–501

Goloubinoff P & De Los Rios P (2007) The mechanism of Hsp70 chaperones: (entropic) pulling the models together. *Trends Biochem Sci* 32: 372–380

Hipp MS, Kasturi P & Hartl FU (2019) The proteostasis network and its decline in ageing. *Nat Rev Mol Cell Biol* 20: 421–435

Holec SAM & Woerman AL (2021) Evidence of distinct α-synuclein strains underlying disease heterogeneity. *Acta Neuropathol* 142: 73–86

Hoppe SO, Uzunoğlu G & Nussbaum-Krammer C (2021) α-Synuclein Strains: Does Amyloid Conformation Explain the Heterogeneity of Synucleinopathies? *Biomolecules* 11

Hoyer W, Antony T, Cherny D, Heim G, Jovin TM & Subramaniam V (2002) Dependence of α-synuclein aggregate morphology on solution conditions. *J Mol Biol* 322: 383–393

Ikenoue T, Lee Y-H, Kardos J, Saiki M, Yagi H, Kawata Y & Goto Y (2014) Cold Denaturation of α-Synuclein Amyloid Fibrils. *Angewandte Chemie International Edition* 53: 7799–7804

Jucker M & Walker LC (2018) Propagation and spread of pathogenic protein assemblies in neurodegenerative diseases. *Nat Neurosci* 21: 1341–1349

Kim H-Y, Cho M-K, Riedel D, Fernandez CO & Zweckstetter M (2008) Dissociation of Amyloid Fibrils of α-Synuclein in Supercooled Water. *Angewandte Chemie International Edition* 47: 5046–5048

Landureau M, Redeker V, Bellande T, Eyquem S & Melki R (2021) The differential solvent exposure of N-terminal residues provides 'fingerprints' of alpha-synuclein fibrillar polymorphs. *Journal of Biological Chemistry* 296

Li W, West N, Colla E, Pletnikova O, Troncoso JC, Marsh L, Dawson TM, Jäkälä P, Hartmann T, Price DL, *et al* (2005) Aggregation promoting C-terminal truncation of α-synuclein is a normal cellular process and is enhanced by the familial Parkinson's disease-linked mutations. *Proc Natl Acad Sci U S A* 102: 2162–2167

Liu CW, Giasson BI, Lewis KA, Lee VM, DeMartino GN & Thomas PJ (2005) A precipitating role for truncated α-synuclein and the proteasome in α-synuclein aggregation: Implications for pathogenesis of parkinson disease. *Journal of Biological Chemistry* 280: 22670–22678

De Los Rios P, Ben-Zvi A, Slutsky O, Azem A & Goloubinoff P (2006) Hsp70 chaperones accelerate protein translocation and the unfolding of stable protein aggregates by entropic pulling. *Proc Natl Acad Sci U S A* 103: 6166–6171

Makky A, Bousset L, Polesel-Maris J & Melki R (2016) Nanomechanical properties of distinct fibrillar polymorphs of the protein α-synuclein. *Sci Rep* 6

Marrero-Winkens C, Sankaran C & Schätzl HM (2020) From Seeds to Fibrils and Back: Fragmentation as an Overlooked Step in the Propagation of Prions and Prion-Like Proteins. *Biomolecules* 10

De Mattos EP, Wentink A, Nussbaum-Krammer C, Hansen C, Bergink S, Melki R & Kampinga HH (2020) Protein Quality Control Pathways at the Crossroad of Synucleinopathies. *J Parkinsons Dis* 10: 369–382

McCann H, Stevens CH, Cartwright H & Halliday GM (2014) α-Synucleinopathy phenotypes. *Parkinsonism Relat Disord* 20: S62–S67

Nachman E, Wentink AS, Madiona K, Bousset L, Katsinelos T, Allinson K, Kampinga H, McEwan WA, Jahn TR, Melki R, *et al* (2020) Disassembly of Tau fibrils by the human Hsp70 disaggregation machinery generates small seeding-competent species. *J Biol Chem* 295: 9676–9690

Nillegoda NB, Kirstein J, Szlachcic A, Berynskyy M, Stank A, Stengel F, Arnsburg K, Gao X, Scior A, Aebersold R, *et al* (2015) Crucial HSP70 co-chaperone complex unlocks metazoan protein disaggregation. *Nature* 524: 247–251

Nury C, Redeker V, Dautrey S, Romieu A, Van Der Rest G, Renard PY, Melki R & Chamot-Rooke J (2015) A novel bio-orthogonal cross-linker for improved protein/protein interaction analysis. *Anal Chem* 87: 1853–1860

Peelaerts W, Bousset L, Van Der Perren A, Moskalyuk A, Pulizzi R, Giugliano M, Van Den Haute C, Melki R & Baekelandt V (2015) α-Synuclein strains cause distinct synucleinopathies after local and systemic administration. *Nature* 522: 340–344

Peng C, Gathagan RJ, Covell DJ, Medellin C, Stieber A, Robinson JL, Zhang B, Pitkin RM, Olufemi MF, Luk KC, *et al* (2018) Cellular milieu imparts distinct pathological α-synuclein strains in α-synucleinopathies. *Nature* 557: 558–563

Van der Perren A, Gelders G, Fenyi A, Bousset L, Brito F, Peelaerts W, Van den Haute C, Gentleman S, Melki R & Baekelandt V (2020) The structural differences between patient-derived α-synuclein strains dictate characteristics of Parkinson's disease, multiple system atrophy and dementia with Lewy bodies. *Acta Neuropathol* 139: 977–1000

Redeker V, Pemberton S, Bienvenut W, Bousset L & Melki R (2012) Identification of protein interfaces between alpha-synuclein, the principal component of Lewy bodies in Parkinson disease, and the molecular chaperones human Hsc70 and the yeast Ssa1p. *J Biol Chem* 287: 32630–32639

Saha I, Yuste-Checa P, Da Silva Padilha M, Guo Q, Körner R, Holthusen H, Trinkaus VA, Dudanova I, Fernández-Busnadiego R, Baumeister W, *et al* (2023) The AAA+ chaperone VCP disaggregates Tau fibrils and generates aggregate seeds in a cellular system. *Nat Commun* 14

Sanders DW, Kaufman SK, DeVos SL, Sharma AM, Mirbaha H, Li A, Barker SJ, Foley AC, Thorpe JR, Serpell LC, *et al* (2014) Distinct Tau Prion Strains Propagate in Cells and Mice and Define Different Tauopathies. *Neuron* 82: 1271–1288

Schneider MM, Gautam S, Herling TW, Andrzejewska E, Krainer G, Miller AM, Trinkaus VA, Peter QAE, Ruggeri FS, Vendruscolo M, *et al* (2021) The Hsc70 disaggregation machinery removes monomer units directly from α-synuclein fibril ends. *Nat Commun* 12

Schweighauser M, Shi Y, Tarutani A, Kametani F, Murzin AG, Ghetti B, Matsubara T, Tomita T, Ando T, Hasegawa K, *et al* (2020) Structures of α-synuclein filaments from multiple system atrophy. *Nature* 585: 464–469

Scior A, Buntru A, Arnsburg K, Ast A, Iburg M, Juenemann K, Pigazzini ML, Mlody B, Puchkov D, Priller J, *et al* (2018) Complete suppression of Htt fibrilization and disaggregation of Htt fibrils by a trimeric chaperone complex. *EMBO J* 37

Shahnawaz M, Mukherjee A, Pritzkow S, Mendez N, Rabadia P, Liu X, Hu B, Schmeichel A, Singer W, Wu G, *et al* (2020) Discriminating alpha-synuclein strains in Parkinson's disease and multiple system atrophy. *Nature* 578: 273–277

Spillantini MG, Crowther RA, Jakes R, Cairns NJ, Lantos PL & Goedert M (1998) Filamentous a-synuclein inclusions link multiple system atrophy with Parkinson's disease and dementia with Lewy bodies. *Neurosci Lett* 251: 205–208

Spillantini MG, Schmidt ML, Lee VM-Y, Trojanowski JQ, Jakes R & Goedert M (1997) α-Synuclein in Lewy bodies. *Nature* 388: 839–840

Taguchi Y V, Gorenberg EL, Nagy M, Thrasher D, Fenton WA, Volpicelli-Daley L, Horwich AL & Chandra SS (2019) Hsp110 mitigates alpha-synuclein pathology in vivo. *Proc Natl Acad Sci U S A* 116: 24310–24316

Tittelmeier J, Druffel-Augustin S, Alik A, Melki R & Nussbaum-Krammer C (2022) Dissecting aggregation and seeding dynamics of α-Syn polymorphs using the phasor approach to FLIM. *Commun Biol* 5: 1345

Tittelmeier J, Nachman E & Nussbaum-Krammer C (2020) Molecular Chaperones: A Double-Edged Sword in Neurodegenerative Diseases. *Front Aging Neurosci* 12

Wakabayashi K, Yoshimoto M, Tsuji S & Takahashi H (1998) a-Synuclein immunoreactivity in glial cytoplasmic inclusions in multiple system atrophy. *Neurosci Lett* 249: 180–182

Wentink A, Nussbaum-Krammer C & Bukau B (2019) Modulation of Amyloid States by Molecular Chaperones. *Cold Spring Harb Perspect Biol* 11

Wentink A & Rosenzweig R (2023) Protein disaggregation machineries in the human cytosol. *Curr Opin Struct Biol* 83

Wentink AS, Nillegoda NB, Feufel J, Ubartaitė G, Schneider CP, De Los Rios P, Hennig J, Barducci A & Bukau B (2020) Molecular dissection of amyloid disaggregation by human HSP70. *Nature* 587: 483–488

Woerman AL & Bartz JC (2024) Effect of host and strain factors on α-synuclein prion pathogenesis. *Trends Neurosci* 47

Yang Y, Shi Y, Schweighauser M, Zhang X, Kotecha A, Murzin AG, Garringer HJ, Cullinane PW, Saito Y, Foroud T, *et al* (2022) Structures of α-synuclein filaments from human brains with Lewy pathology. *Nature* 610: 791–795

Zhang Z, Kang SS, Liu X, Ahn EH, Zhang Z, He L, Iuvone PM, Duong DM, Seyfried NT, Benskey MJ, *et al* (2017) Asparagine endopeptidase cleaves α-synuclein and mediates pathologic activities in Parkinson's disease. *Nat Struct Mol Biol* 24: 632–642

Figure Legends:

Figure 1 | α-syn fibrillar polymorphs show differences in disaggregation kinetics by the human Hsp70 chaperone machinery. A Negative stain EM images of α-syn fibrillar polymorphs XG, FM, Ri, F65 and F91 (left) and the C-terminally truncated F110 (right) (scale bar 200 nm). The corresponding α-syn sequence is indicated above. **B** Representative immunoblot of supernatant (S) and pellet (P) fractions after a 16 h disaggregation reaction of α-syn polymorphs incubated with the active (+ ATP) and inactive (- ATP) chaperone machinery (Hsc70, DnaJB1, Apg2). **C** Quantification of released α-syn proteins in the supernatant as a fraction of the total (P + S) after 16h disaggregation by the active chaperone machinery. **D** Representative data of a Thioflavin T (ThT) based disaggregation assay of the polymorphs (XG, blue; F91, red; F65, green; FM, yellow; Ri, grey; F110, purple) by the human Hsc70 chaperone machinery. **E** Percentage of disaggregation, calculated from ThT assays, after 16 h disaggregation of the different fibrillar polymorphs by the Hsc70 machinery. Data are mean ± s.e.m. Individual datapoints represent the mean of three technical replicates for independent biological replicates (fibril batches).

Figure 2 | Differences in polymorph structures affect interactions with the chaperone machinery. A Steady-state anisotropy titration of AF-594-labelled DnaJB1 with different concentrations of α-syn fibril polymorphs (XG; blue, FM; orange, Ri; gray, F65; green, F91; red, F110; purple). **B** Correlation of experimentally determined DnaJB1 dissociation constants and disaggregation efficiency (as determined in Fig. 1E) including (dotted line) and excluding (solid line) polymorph Ri. **C** Steady-state anisotropy titration experiment of AF-488 labelled Hsc70 in the presence of DnaJB1 and 2 mM ATP from α-syn fibril polymorphs. **D** Correlation of experimentally determined Hsc70 dissociation constants and disaggregation efficiency (as determined in Fig 1.E) including (dotted line) and excluding (solid line) polymorph Ri. Data are mean ± s.e.m.

Figure 3 |Fibrillar fragments accumulate to various degrees during chaperone mediated disaggregation of α-syn polymorphs. A Representative sucrose density gradient (10-85 %) profile (AF555 fluorescence signal) of the reaction mixture after incubation of AF555-labeled fibrils with the active chaperone machinery (Hsc70, DnaJB1, Apg2, + ATP) for 20 min, 2 h, 16 h, and incubation with the inactive machinery (No Disagg, -ATP) of polymorphs F65, FM and Ri. **B** Relative abundance of fibrils (orange), small fragments/oligomers (blue), and monomers (red) in the reaction mixtures of the specified polymorphs (XG; FM; Ri; F65; F91; F100) at indicated timepoint during the disaggregation reaction. The relative abundance was calculated by integration of the monomer (fractions 0-2), small

fragment/oligomer (fractions 3-10), or fibril peaks (fractions 12-20) of the sucrose gradient plot divided by the total. Three individual biological replicates (△, □, ○) are plotted with a connecting line.

Figure 4 | Disaggregation of fibrils produce seeding competent fragments *in vitro*.

A Representative aggregation curves of α-syn monomers seeded with Fibrils (orange); No Disaggregation (black), Disaggregation (green), No seed (grey) and only chaperones (purple) samples for the polymorphs FM (left) and F65 (right). **B** Quantification of the initial rate of the seeded reaction in A, normalized to the fibril only reactions. **C** Centrifugation procedure to separate different disaggregation reaction products. A total disaggregation reaction is centrifuged at 3,600g for 15 min, fibrils (orange) are separated in the pellet and small fragments/oligomers remain in the supernatant (left). By centrifugation of the total reaction at a higher speed (435,630g) for 30 min, small fragments/oligomers (blue) and fibrils are pelleted and only monomers (red) remain in the supernatant (right). **D** Representative EM images of a disaggregation and No disaggregation reaction (total reaction; middle), small fragments/oligomer fraction (left) and monomer fraction (right); scale bar 500 nm. **E** Representative aggregation curves of α-syn monomers seeded with a total disaggregation reaction (green) and fractionated small fragments/oligomer (blue) and monomer (red) fraction of polymorph FM (left) and F65 (right). **F** Initial rate of seeded reaction. Data are mean ± s.e.m. **G** Representative aggregation curves of α-syn monomers seeded with fractions of a non-disaggregated (-ATP) reaction mixture (total, green; fragments/oligomer, blue; monomer, red). **H** Quantification of initial rate of seeded reactions as shown in G normalized to the total disaggregation reactions. Data are mean ± s.e.m.

Figure 5 | Disaggregation reaction products trigger foci formation in a human cell model. A Experimental setup of an *in cellulo* seeding assay. Three different reaction mixtures are analysed after 16 hours incubation at 30 °C; fibrils only (Fibrils), fibrils incubated with the chaperone machinery (Hsc70, DnaJB1, Apg2) in the absence (No Disaggregation), and presence of ATP (Disaggregation). In addition, the disaggregation sample is further fractionated by differential centrifugation as described in Fig. 4C to generate "Fragments/Oligomers" and "Monomers" fractions. The reaction mixtures are added as seeds to HEK293T cells stably expressing α-syn A53T-YFP and the number of cells with fluorescent foci are counted. **B** Representative fluorescence microscopy images of reporter HEK293T cells seeded with treated fibrils of polymorphs FM and F65. Untreated cells are shown in the lower right (scale bar 20 µm). Fibrils only, fibrils incubated with chaperones in the absence (No Disaggregation) and presence of ATP (Disaggregation), as well as small fragments/oligomer and

monomer fractions of the disaggregation reaction separated by centrifugation as described in Fig. 4. **C** Quantification of cells with foci normalized to the No Disaggregation sample (No Disaggregation, black; Disaggregation, green; small fragments/oligomers, blue; monomers, red; fibrils, orange). Data are mean ± s.e.m. Statistical analysis was performed by nonparametric Two-Way ANOVA with pairwise comparisons of estimated marginal means with Tukey correction for multiple comparisons.

Figure 6 | Disaggregation efficiency is depended on a combination of chaperone binding and fibril stability. A Model of disaggregation efficiency (green) as a function of fibril stability (y-axis) and chaperone binding (x-axis). The interplay between chaperone binding to the fibrils and fibril stability has to be in the indicated green area for efficient disaggregation, whereas fibrils located in grey areas (high stability and/or low chaperone binding) are resistant to disaggregation. The distribution of fibril polymorphs analysed in this study are shown in the plot on the right. **B** Cartoon representation of *in vitro* aggregated α-syn polymorph FM, Ri and F91. The monomeric α-syn sequence consisting of N-terminal domain, NAC-region, and C-terminal domain with indicated chaperone binding sites (Hsc70, blue; DnaJB1, red) based on Wentink *et al,* 2020 (top). Known regions of the monomeric α-syn sequence in the polymorphs that are incorporated into the amyloid core (big arrow), β-sheet structures (small arrow)(Hoppe *et al*, 2021; Landureau *et al*, 2021). In particular, the N-terminal region varies in the degree of structure observed between the various polymorphs, coinciding with the proposed binding sites of Hsc70.

Figure 1

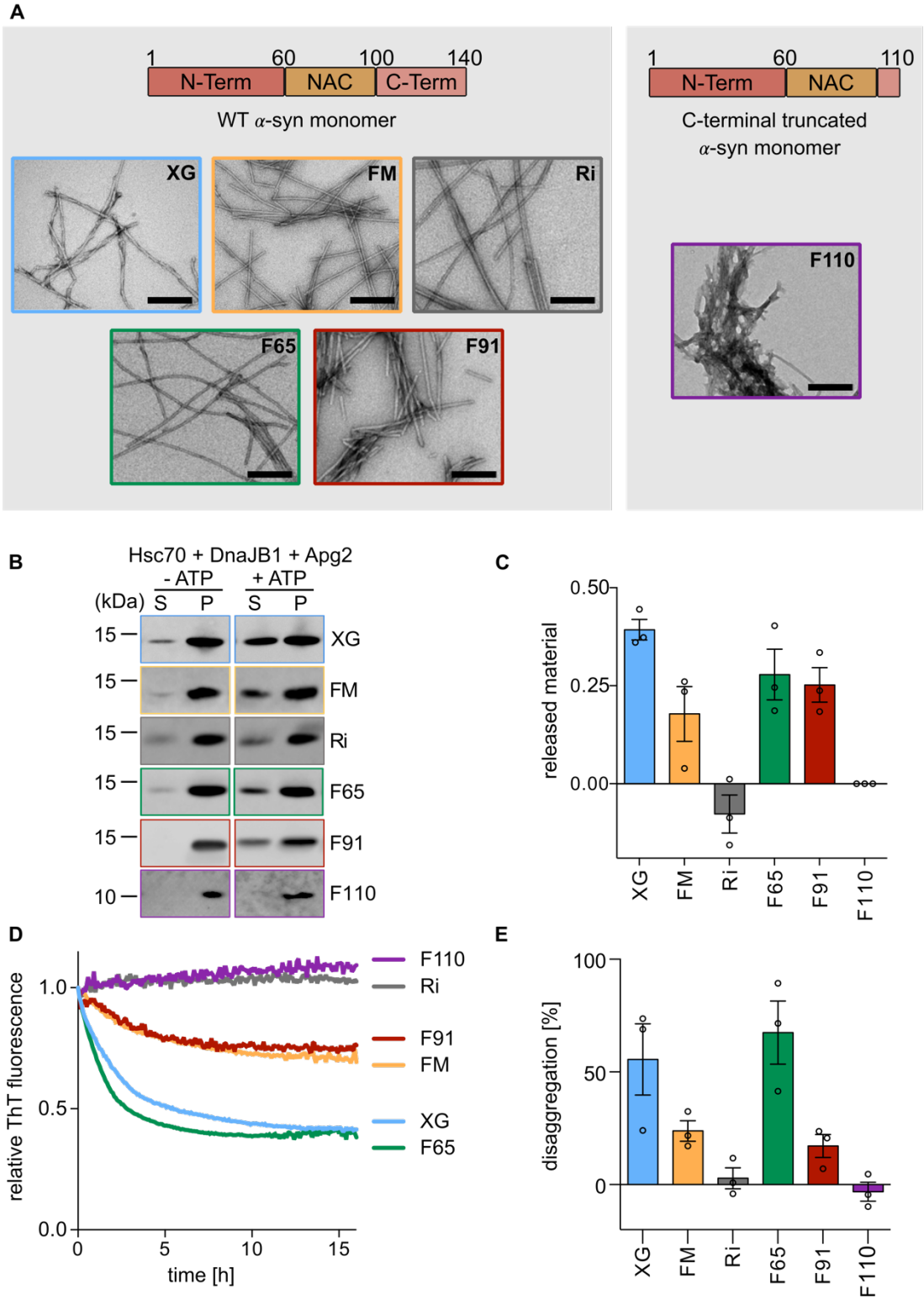
A
1
60
100
140
N-Term
NAC
C-Term
WT α-syn monomer
XG
FM
Ri
F65
F91
1
60
110
N-Term
NAC
C-terminal truncated
α-syn monomer
F110
B
Hsc70 + DnaJB1 + Apg2
- ATP
+ ATP
(kDa)
S
P
S
P
15
15
15
15
15
10
XG
FM
Ri
F65
F91
F110
C
released material
0.50
0.25
0.00
XG
FM
Ri
F65
F91
F110
D
relative ThT fluorescence
1.0
0.5
0.0
0
5
10
15
time [h]
F110
Ri
F91
FM
XG
F65
E
disaggregation [%]
100
50
0
XG
FM
Ri
F65
F91
F110

Figure 2

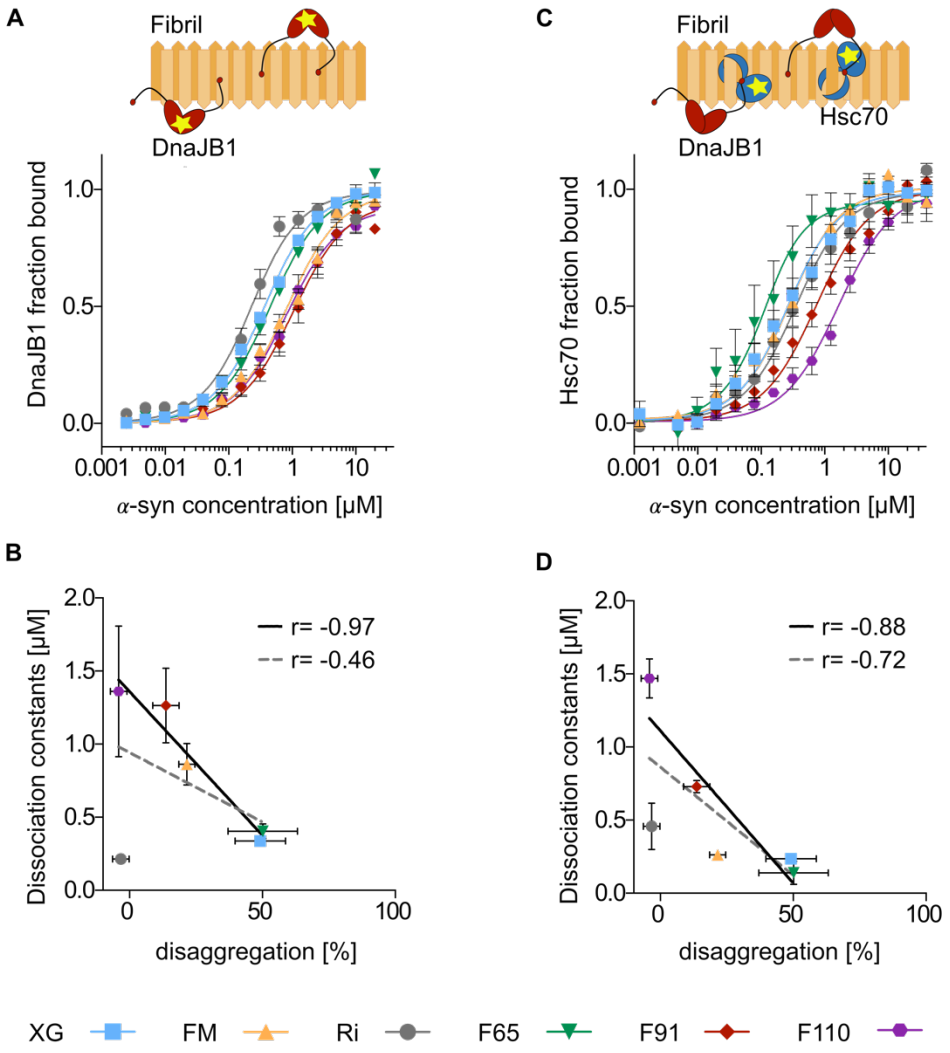
A
Fibril
DnaJB1
DnaJB1 fraction bound
1.0
0.5
0.0
0.001
0.01
0.1
1
10
α-syn concentration [μM]
C
Fibril
Hsc70
DnaJB1
Hsc70 fraction bound
1.0
0.5
0.0
0.001
0.01
0.1
1
10
α-syn concentration [μM]
B
Dissociation constants [μM]
2.0
1.5
1.0
0.5
0.0
r= -0.97
r= -0.46
0
50
100
disaggregation [%]
D
Dissociation constants [μM]
2.0
1.5
1.0
0.5
0.0
r= -0.88
r= -0.72
0
50
100
disaggregation [%]
XG
FM
Ri
F65
F91
F110

Figure 3

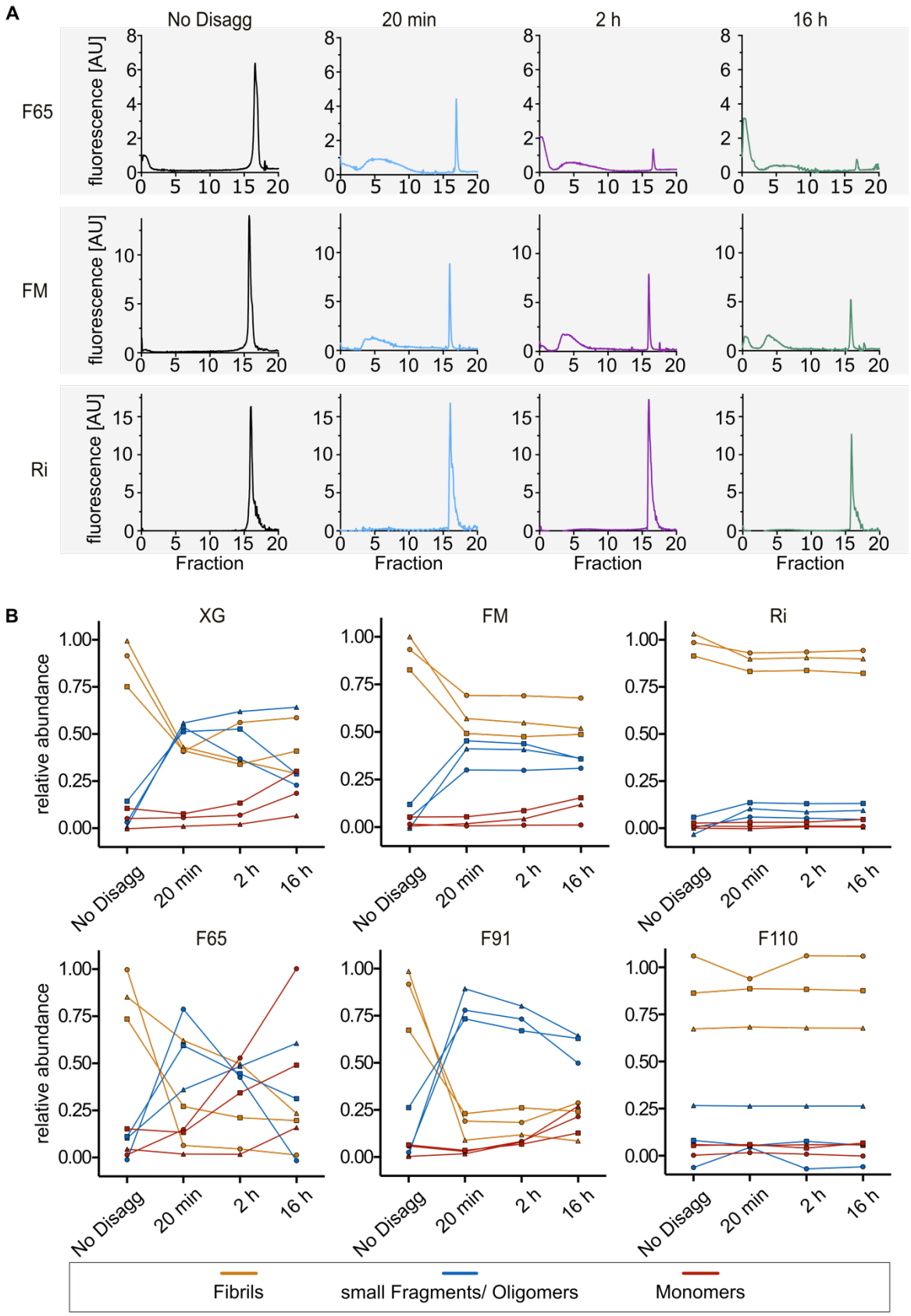
A
No Disagg
20 min
2 h
16 h
F65
FM
Ri
fluorescence [AU]
Fraction
B
XG
FM
Ri
F65
F91
F110
relative abundance
No Disagg
20 min
2 h
16 h
Fibrils
small Fragments/ Oligomers
Monomers

Figure 4

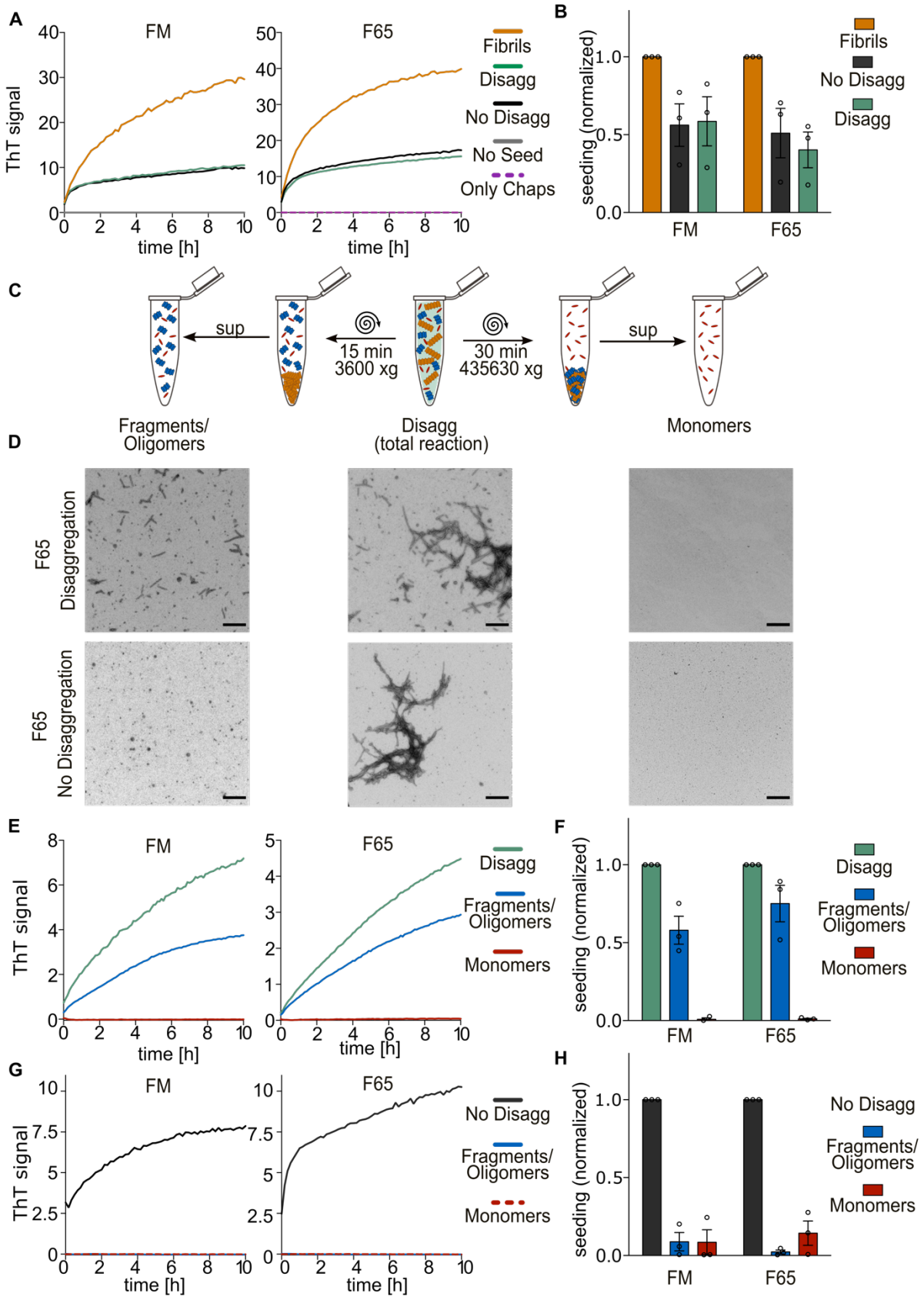
A
FM
F65
ThT signal
time [h]
Fibrils
Disagg
No Disagg
No Seed
Only Chaps
B
seeding (normalized)
FM
F65
Fibrils
No Disagg
Disagg
C
sup
15 min
3600 xg
30 min
435630 xg
sup
Fragments/
Oligomers
Disagg
(total reaction)
Monomers
D
F65
Disaggregation
F65
No Disaggregation
E
FM
F65
ThT signal
time [h]
Disagg
Fragments/
Oligomers
Monomers
F
seeding (normalized)
FM
F65
Disagg
Fragments/
Oligomers
Monomers
G
FM
F65
ThT signal
time [h]
No Disagg
Fragments/
Oligomers
Monomers
H
seeding (normalized)
FM
F65
No Disagg
Fragments/
Oligomers
Monomers

Figure 5

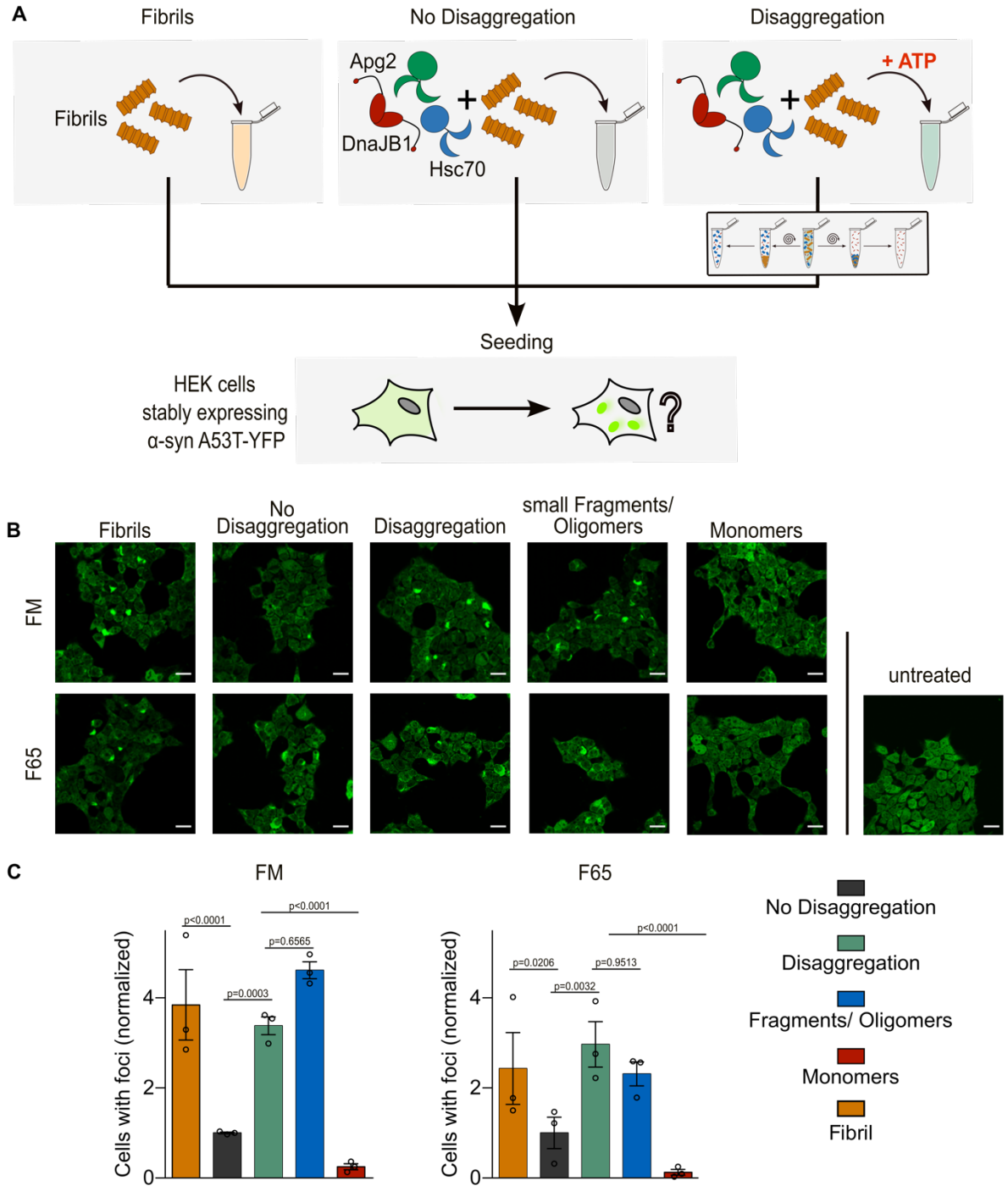
A
Fibrils
No Disaggregation
Disaggregation
Fibrils
Apg2
DnaJB1
Hsc70
+ ATP
Seeding
HEK cells
stably expressing
α-syn A53T-YFP
B
Fibrils
No Disaggregation
Disaggregation
small Fragments/ Oligomers
Monomers
FM
F65
untreated
C
FM
F65
Cells with foci (normalized)
p<0.0001
p=0.0003
p=0.6565
p<0.0001
p=0.0206
p=0.0032
p=0.9513
p<0.0001
No Disaggregation
Disaggregation
Fragments/ Oligomers
Monomers
Fibril

Figure 6

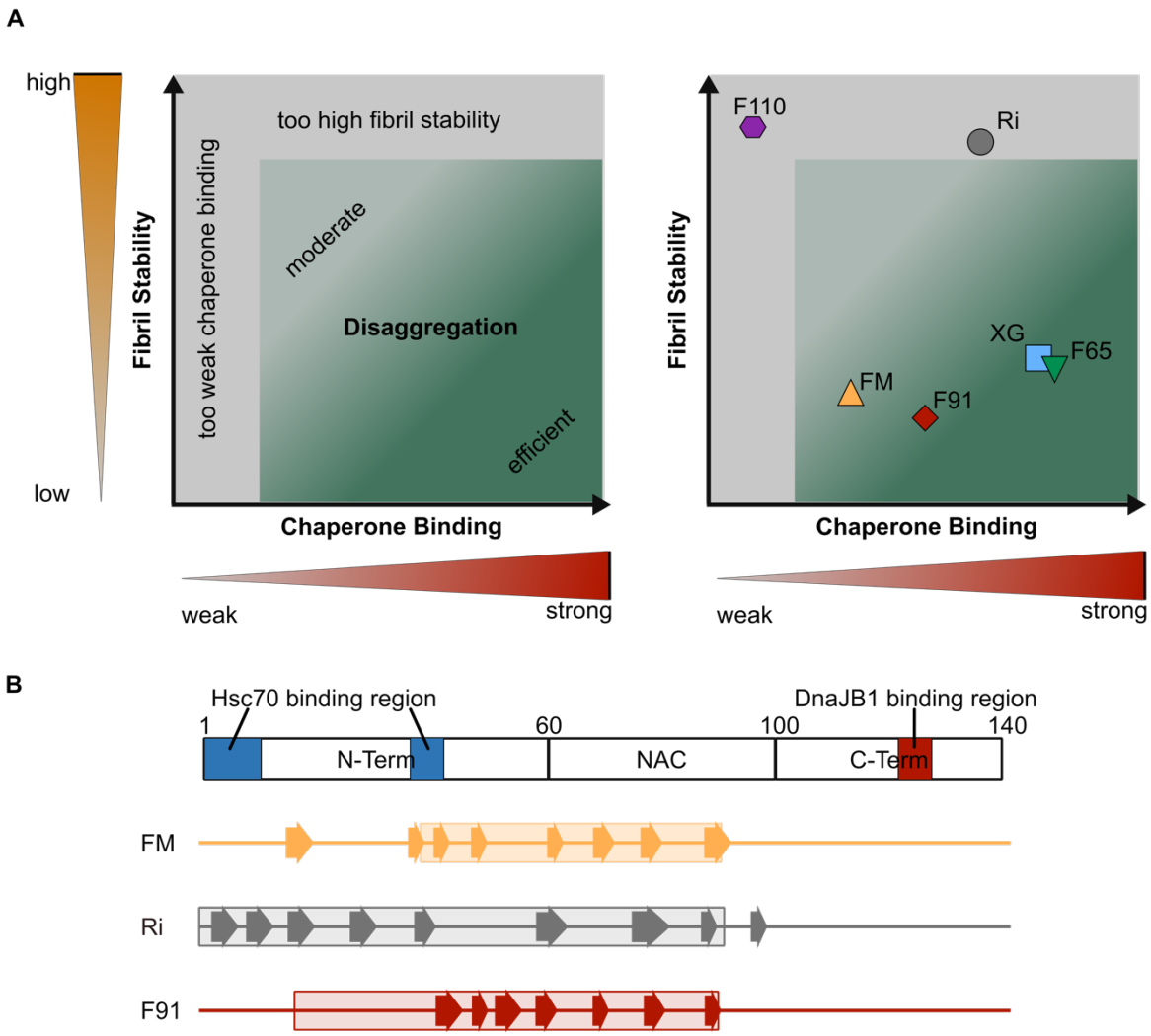
A
high
low
Fibril Stability
too high fibril stability
too weak chaperone binding
moderate
Disaggregation
efficient
Chaperone Binding
weak
strong
F110
Ri
XG
F65
FM
F91
Fibril Stability
Chaperone Binding
weak
strong
B
Hsc70 binding region
DnaJB1 binding region
1
60
100
140
N-Term
NAC
C-Term
FM
Ri
F91